Journal of Solid State Chemistry **152,** 87–98 (2000)
doi:10.1006/jssc.2000.8672, available online at http://www.idealibrary.com on IDEAL®

Microporous Porphyrin and Metalloporphyrin Materials

Margaret E. Kosal and Kenneth S. Suslick

School of Chemical Sciences, University of Illinois at Urbana-Champaign, Urbana, Illinois 61801

The diverse efforts to rationally construct microporous solids using porphyrins and metalloporphyrins as molecular building blocks are reviewed. Porphyrin-based molecular crystals, hydrogen-bonded networks, and metal ion coordination polymer networks are examined in detail. Recurring geometrical motifs observed in the structural frameworks of different porphyrinic solids are emphasized, and the influences of solvates and guest molecules are explored. Attempts to construct porphyrin–siloxane networks are also reviewed. © 2000 Academic Press

Key Words: **porphyrins; metalloporphyrins; microporous materials; crystal engineering; solid-state networks.**

INTRODUCTION

Porphyrins and related macrocycles provide an extremely versatile synthetic base for a variety of materials applications. The exploration of metalloporphyrin assemblies as building blocks for tailored materials properties has found rapid growth during the past decade (1). A number of researchers have explored synthetic strategies for the construction of porphyrinic solids that contain molecularly sized cavities or channels. Porphyrin macrocycles can be envisioned as flat, rigid, geometrically square building blocks approximately 1 nm wide. The out-of-plane twist of *meso*-substituents on the porphyrin periphery (as necessitated by steric constraints) provides a route for constructing structures extending beyond the porphyrin macrocycle plane. Chemical modification of the perimeter is facile in many cases. Additionally, the thermal and chemical stability of porphyrins makes them attractive precursors for potential uses at elevated temperatures. Furthermore, metalloporphyrins have demonstrated catalytic ability in a wide variety of reactions (2, 3), especially oxidative processes; thus, porous metalloporphyrin networks have the potential to act as shape- and size-selective heterogeneous catalysts.

MOLECULAR PORPHYRIN STRUCTURES

Strouse and coworkers (4–6) examined the extensive crystal structure library of free base and metalated porphyrin lattice clathrates in which the predominant intermolecular bonding interactions are weak molecular van der Waals forces. In addition to H_2(TPP) (Table 1), their database included simple substituted porphyrins such as *o*-amino-(H_2(T(*o*-NH_2)PP)), *p*-methoxy-(H_2(T(*p*-OCH_3)PP)), and *p*-bromo-(H_2(T(*p*-Br)PP)) tetraphenylporphyrins. While the most commonly studied metalloporphyrin was the Zn(II) species, at least 11 other metalloporphyrins were examined. They realized that the large majority of these structures contained a high concentration of solvates and were in effect "porphyrin sponges."

The solids of these TPP derivatives generally pack in simple body-centered-cubic (BCC) arrangements. In this non-close-packed arrangement, the porphyrin molecules occupy corners of an imaginary cube with intersecting channels between the porphyrins passing through the center of the cube. The driving force for clathrate formation was identified as the efficient packing of the porphyrin moieties in two dimensions, while the third dimension was accessible for inclusion of guest molecules. The dominant porphyrin–porphyrin interactions were actually between perpendicularly oriented phenyl groups on adjacent tetraarylporphyrins. Similar packing modes were observed for over 65 different TPP species (4).

Channels of solvate molecules exist between chains of parallel TPP molecules (Fig. 1). Estimates of the size of channel width were based on the *d*(002) lattice parameter, corresponding to roughly half of the face to face porphyrin separation. The axial coordination sites (perpendicular to the porphyrin macrocyclic rings) line the edge of the channels. In the free base and four-coordinate metalloporphyrin materials, the most commonly observed ratio was two guest molecules per porphyrin molecule; notable exceptions were in cases of large solvate molecules (i.e., *p*-xylene or phenanthracene). Two axial ligands occupy the channels in six-coordinate metalloporphyrins; and, in the five-coordinate materials, a single axial ligand and a single guest molecule were observed to fill alternately the voids (Fig. 2). This is cited as an example of "programmability" in design of the clathrate materials. Porphyrin to guest ratios as high as 1:5

0022-4596/00 $35.00

TABLE 1
Abbreviations

T(2′,6′-DHP)P	5,10,15,20-Octakis(2,6-dihydroxyphenyl)porphyrinate
T(3,5-CO_2H)PP	5,10,15,20-Tetrakis(3,5-dicarboxyphenyl)porphyrinate
T(3′,5′-DHP)P	5,10,15,20-Octakis(3,5-dihydroxyphenyl)porphyrinate
T(*o*-NH_2)PP	5,10,15,20-Tetra(2-aminophenyl)porphyrinate
T(*p*-Br)PP	5,10,15,20-Tetra(4-bromophenyl)porphyrinate
T(*p*-Cl)PP	5,10,15,20-Tetra(4-chlorophenyl)porphyrinate
T(*p*-CN)PP	5,10,15,20-Tetra(4-cyanophenyl)porphyrinate
T(*p*-CO_2H)PP	5,10,15,20-Tetra(4-carboxy)phenylporphyrinate
T(*p*-F)PP	5,10,15,20-Tetra(4-fluorophenyl)porphyrinate
T(F_5P)P	5,10,15,20-Tetrakis(pentafluorophenyl)porphyrinate
T(*p*-NO_2)PP	5,10,15,20-Tetra(4-nitrophenyl)porphyrinate
T(*p*-OCH_3)PP	5,10,15,20-Tetra(4-methoxyphenyl)porphyrinate
T(*p*-OH)PP	5,10,15,20-Tetra(4-hydroxyphenyl)porphyrinate
TGA	Thermogravimetric analysis
THF	Tetrahydrofuran
TMAP	5,10,15,20-Tetra(5-trimethylaminopentyl)porphyrinate
TMP	5,10,15,20-Tetramethylporphyrinate
TMPyP	5,10,15,20-Tetra(4-*N*-methylpyridinium)porphyrinate
TPP	5,10,15,20-Tetraphenylporphyrinate
TPyP	5,10,15,20-Tetra-*p*-pyridylporphyrinate

were observed for $Mn^{III}(TPP)(CH_3OH)_2(SbCl_6^-)(C_2Cl_4H_2)_2$, which also has multiple channels (5).

Channel width was observed generally to be on the order of 3.4–6.6 Å. Some of the smallest guest filled channels were observed in the Zn(TPP)·2 *m*-fluoronitrobenzene, Zn(TPP)·2 2,4-dinitrobenzene, and Zn(TPP)·2 acridine

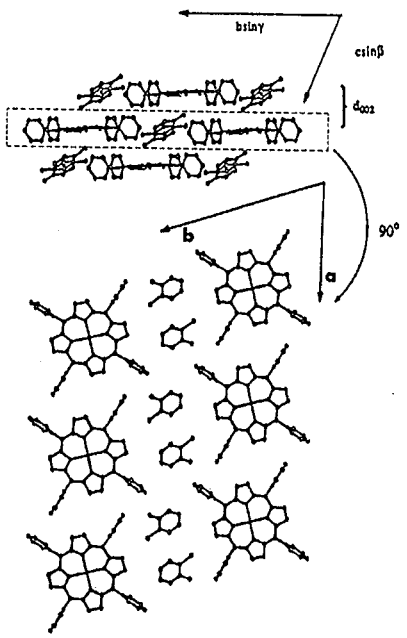

FIG. 1. Porphyrin and guest packing in a typical porphyrin sponge. Reprinted with permission from M. P. Byrn, C. J. Curtis, Y. Hsiou, S. I. Khan, P. A. Sawin, S. K. Tendick, A. Terzis, and C. E. Strouse, *J. Am. Chem. Soc.* **115,** 9480 (1993). Copyright 1993 American Chemical Society.

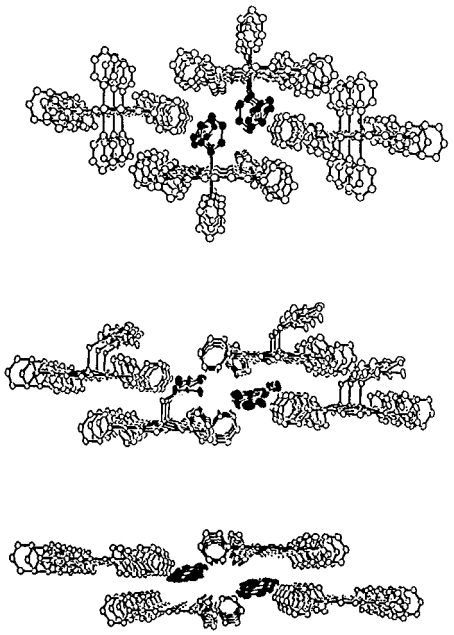

FIG. 2. Basic packing motif for porphyrin clathrates in six-, five-, and four-coordinate TPP complexes. Reprinted with permission from M. P. Byrn, C. J. Curtis, I. Goldberg, Y. Hsiou, S. I. Khan, P. A. Sawin, S. K. Tendick, and C. E. Strouse, *J. Am. Chem. Soc.* **113,** 6549 (1991). Copyright 1991 American Chemical Society.

systems—all which had channel widths calculated at less than 4 Å. The largest spacing for a "normal" clathrate material was observed for $Ru^{II}(TPP)((Ph_2P)_2Me)_2 \cdot CH_2Cl_2$ (5). Layered materials with *d*(002) spacing of 6.8 Å were observed for $Rh^{III}(TPP)(CNCH_2C_6H_5)(PF_6^-)_2$ in which a single layer of guest molecules is located between a double layer of the host porphyrin species, and an even larger *d*(002) spacing of 7.8 Å was noted for a material with a double layer of host $Ce^{IV}(TPP)^{+2}$ separated by another double layer of phthalocyanine molecules and $SbCl_6^-$ anions (6).

The forces holding these solids together, however, are very weak. Consequently, upon removal of solvent, rapid structural changes to a different crystalline phase or to an amorphous material typically occur. In rare cases, exposure of the desolvated solid to vapor of the guest molecule can produce a solid with an X-ray diffraction powder pattern similar to that of the crystalline clathrate materials grown in solution.

Goldberg and coworkers have synthesized porphyrinic solids that utilize other weak intermolecular interactions between porphyrin building blocks. The structures of inclusion compounds formed from halogen substituted tetraphenylporphyrins displayed three general motifs. The most commonly observed patterns involve halogen–halogen attractions between the halo-substituted phenyl groups and attractions between halogen atoms and β-pyrrole hydrogen atoms; these can lead to both one- and two-dimensional arrays (Fig. 3). Inclusion compounds of this variety

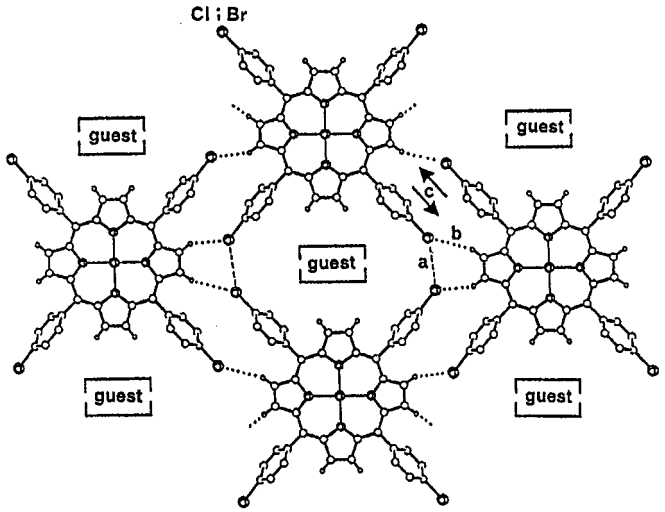

FIG. 3. Schematic of interporphyrin interactions in *p*-chloro- and *p*-bromo-substituted TPPs. Reprinted from P. Dastidar, H. Krupitsky, Z. Stein, and I. Goldberg, *J. Incl. Phenom. Mol. Recog. Chem.* **24,** 241 (1996), Copyright Kluwer Academic Publishers, with kind permission from Kluwer Academic Publishers.

were observed for Zn(T(*p*-Cl)PP) species with guaiacol, nitrobenzene, DMSO, methyl salicylate, (7) methyl phenylacetate, mesitylene, ethyl benzoate, and acetophenone as guests (8) and Zn(T(*p*-Br)PP) species with benzylacetate, methyl salicylate, ethyl benzoate, bromobenzene, or *p*-xylene as guests (9). The intermolecular Cl ··· Cl distance defines the width of the guest cavities. The Cl ··· Cl separation of 3.63 Å reported for Zn(T(*p*-Cl)PP)·$C_7H_8O_2$ is typical of the 1:1 inclusion complexes; values for 1:2 inclusion compounds such as Zn(T(*p*-Cl)PP)·$2C_2H_6OS$ (3.90 Å) were higher (7). Slightly offset stacking of the porphyrin macrocycles in subsequent layers defined the depth of the cavities. The intermolecular Br ··· Br contact distances were reported as 3.837 Å for a 1:2 Zn(T(*p*-Br)PP)·$2C_8H_8O_3$ (methyl salicylate) inclusion material. Thermogravimetric analysis (TGA) was reported for Zn(T(*p*-Br)PP)·$2C_8H_8O_3$, showing a 21% weight loss for loss of solvent (theoretical 23%) at $\sim$125°C without further loss to 350°C (9). In the case of the 1:1 Zn(T(*p*-Cl)PP):nitrobenzene inclusion compound, the observed helical arrangement of the porphyrin backbone produced a polarized cavity environment, with ordering of guest molecules (8). The *p*-xylene clathrate of Zn(T(*p*-F)PP) featured a linear chain structure similar to that noted in the chloro- and bromo- derivatives. However, the nonbonding F ··· F contact distances have increased to 4.1 and 4.2 Å, respectively, characteristic of a repulsive interaction rather than attractive force as observed in other halogenated porphyrin materials (7).

Tightly packed herringbone-like layers characterize a second observed motif (Fig. 4). Structures of this type were observed for Zn(T(*p*-Cl)PP)·C_7H_7Cl (*o*-chlorotoluene) (7), Zn(T(*p*-Br)PP)·$3C_5H_5N$, and Zn(T(*p*-Br)PP)·$4C_9H_{12}$

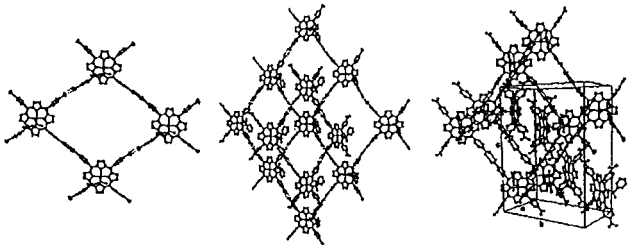

FIG. 4. Herringbone packing arrangement of Zn(T(*p*-OH)PP)·$2C_7H_6O{\cdot}H_2O$. Reprinted from H. Krupitsky, Z. Stein, and I. Goldberg, *J. Incl. Phenom. Mol. Recog. Chem.* **20,** 211 (1995), Copyright Kluwer Academic Publishers, with kind permission from Kluwer Academic Publishers.

(mesitylene) (9). In the *p*-bromo compounds, ligation of two pyridines to the Zn(II) ion was observed. The remaining uncoordinated guest molecules were observed to occupy voids between the porphyrin moieties.

A third motif, also observed in Strouse's TPP materials, has tightly packed corrugated layers in which the guest molecules intercalate between the layers: e.g., Zn(T(*p*-Br)PP)·$4C_6H_7N$ (aniline) and Zn(T(*p*-Br)PP)·$2C_8H_{11}N$ (methylbenzylamine) (Fig. 5) (9).

HYDROGEN-BONDED NETWORKS

In an effort to synthesize more robust frameworks, hydrogen-bond interactions have been explored as the basis for linking porphyrin molecules. Hydrogen bonds offer the

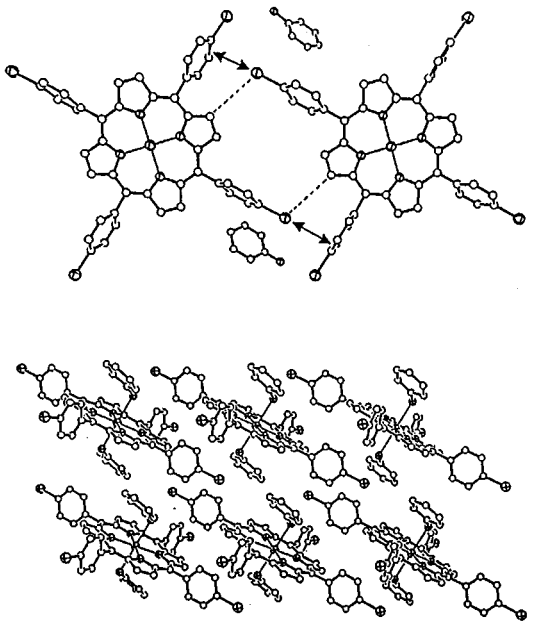

FIG. 5. Corrugated layer arrangement in Zn(T(*p*-Br)PP)·$4C_6H_7N$. Reprinted from P. Dastidar, H. Krupitsky, Z. Stein, and I. Goldberg, *J. Incl. Phenom. Mol. Recog. Chem.* **24,** 241 (1996), Copyright Kluwer Academic Publishers, with kind permission from Kluwer Academic Publishers.

additional advantages of directionality and selectivity (10). While hydrogen bonding is certainly a stronger interaction than the van der Waals interactions that hold the "porphyrin sponge" solids together, even multiple hydrogen bonds per porphyrin still provide only modest stabilization of the solids in the absence of their solvates.

Goldberg and coworkers have explored a number of substituted tetraphenylporphyrins as building blocks for porous solids. Some of the inclusion compounds of 5,10,15,20-tetra(4-hydroxy)phenyl porphyrins (H_2(T(*p*-OH)PP)) featured structures similar to those observed in halogenated species (8). In a motif similar to the previously observed linear polymeric chains, the Zn(T(*p*-OH)PP)$\cdot 2C_6H_6O \cdot 2H_2O$ (phenol), Zn(T(*p*-OH)PP)$\cdot 2C_9H_{10}O \cdot H_2O$ (benzyl acetate), and Zn(T(*p*-OH)PP)$\cdot 2C_7H_6O \cdot H_2O$ (benzaldehyde) clathrate materials are characterized by dual *cis*-side OH $\cdots$ OH intermolecular attractions. There are no intermolecular interactions between *para*-substituted hydroxyl groups and β-pyrrole hydrogen atoms of adjacent linear chains (as observed in the halogenated materials). Instead, *para*-substituted hydroxyl groups hydrogen bond with hydroxyl groups on adjacent linear chains, forming a two-dimensional porphyrin network. A guest water molecule participates in this interchain bonding arrangement. In this manner, two different guest cavities are formed—voids between porphyrins in a polymeric chain and between chains in the two-dimensional array. Layers are stacked in an offset manner, therefore forming pores instead of channels in which axially coordinated ligands partially occupy the voids in successive layers.

Similar *cis*-side OH $\cdots$ OH interactions are observed in the Cu(T(*p*-OH)PP)$\cdot 4C_8H_8O$ (acetophenone), Zn(T(*p*-OH)PP)$\cdot 2C_8H_{10} \cdot 4CH_3OH$ (*o*-xylene and methanol) and Zn(T(*p*-OH)PP)$\cdot 5C_7H_8O_2$ (guaiacol) materials. Guest molecules which hydrogen bond to the hydroxyl groups (Fig. 6) separate the linear porphyrinic chains. In the acetophenone and *o*-xylene included materials, porphyrin macrocyclic planes of successive layers are offset, preventing the formation of distinct channels. The parallel porphyrin macrocycles of successive layers are directly aligned in the guaiacol-included material generating ~ 9 Å cavities. Between layers of porphyrin macrocycles, a single parallel-oriented guest molecule is sandwiched. There is another guest guaiacol molecule situated below the area of hydrogen bonding between porphyrin molecules (8).

For the toluene inclusion solid, Zn(T(*p*-OH)PP)$\cdot 3C_7H_8$, a three-dimensional framework is observed. Hydrogen bonding between *trans*-oriented porphyrin hydroxyl groups and parallel chains form a geometry approximating a body-centered cubic arrangement. Porphyrins within successive layers of *trans*-hydrogen bonded chains have an interlayer separation of 6.5 Å in which a guest molecule resides. Channels perpendicular to the layers of porphyrin chains are observed. The significant translational and rotational disorder of guest species in the crystal structure supports the presence of channels (8).

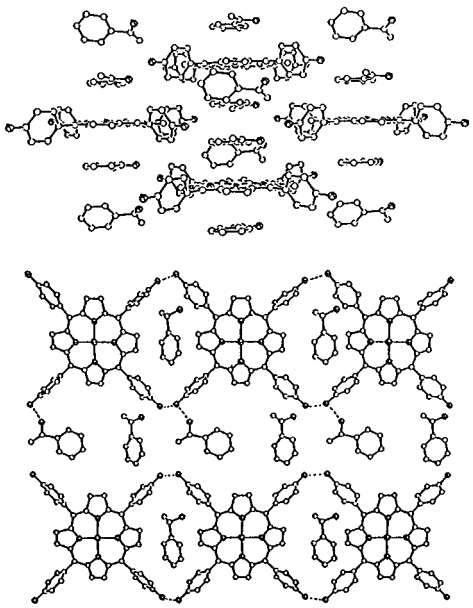

FIG. 6. Layered structure in Cu(T(*p*-OH)PP)$\cdot 4C_8H_8O$ (top); illustration of guest-filled channels in the same material (bottom). Reprinted from I. Goldberg, H. Krupitsky, Z. Stein, Y. Hsiou, and C. E. Strouse, *Supramol. Chem.* **4,** 203 (1995), Copyright OPA, N.V., with permission from Gordon and Breach Publishers.

The clathrate of equimolar 5,10,15,20-tetra(4-methoxy) phenylporphyrinatozinc(II), phenol and water, Zn(T(*p*-OCH_3)PP)$\cdot C_6H_6O \cdot H_2O$, exhibits intermolecular hydrogen-bonding between methoxy substituents and axially coordinated water molecules in successive porphyrin layers. This arrangement generates a three-dimensional cross-linked framework in which phenol molecules occupy cavities between layers of porphyrin molecules similar to results reported for five-coordinate metalated tetraphenylporphyrin inclusion solids by Strouse (4); however, the axial ligand is now available to form weak hydrogen bonds with the *para*-substituent on the phenyl group of a successive layer. A corrugated sheet-like geometry is found in Zn(T(*p*-OCH_3)PP)$\cdot 2C_8H_8O_2$ (*o*-hydroxyacetophenone) material (8).

For clathrates of 5,10,15,20-tetra(4-cyano)phenyl porphyrin, H_2(T(p-CN)PP), four structural motifs were encountered by Goldberg *et al.* (11). The first hydrogen-bonding motif involves open two-dimensional networks in which a cyano group hydrogen bonds to β-hydrogen atoms on an adjacent porphyrin pyrrole ring in a dimeric fashion. The individual [–CN $\cdots$ H–(β-pyrrole)] interactions are described as short (3.41–3.59 Å) and linear, although the two H-bond interactions of the dimer are not parallel to each other. The 1:2 inclusion compound of Cu(T(*p*-CN)PP) with chloroform produced a framework with elliptical interporphyrin cavities (6.4×11 Å), whereas larger square-shaped

cavities (10×10 Å) were observed for Zn(T(*p*-CN)PP) with two larger ethyl benzoate molecules—one axially ligated to the central Zn(II) ion and the other located within the interporphyrin void.

One dimensional chains utilizing similar dimeric interactions were observed for the inclusion solids Zn(T(*p*-CN)PP)$\cdot 3C_7H_8O_2$ (guaiacol) and Zn(T(*p*-CN)PP)$\cdot 2.5C_7H_8O$ (anisole). In the guaiacol-included material, a 20.06×4.1-Å cavity is noted. A similar structure to that observed in *p*-chloro- and *p*-bromo-phenyl-substituted porphyrins (Fig. 3) is observed for Zn(T(*p*-NO_2)PP)$\cdot 3C_{10}H_{12}O_2$ (eugenol) with a large cavity of dimensions 23.34×4.19 Å. Herringbone-type interchain interaction between a single cyano substituent and a β-pyrrole hydrogen atom is characteristic of the third type of pattern observed for *para*-cyanophenyl porphyrin materials again reminiscent of one of the structural patterns observed for the *p*-halogenated phenyl porphyrin molecular species (Fig. 4). Interlayer spacing of 4.3 Å was observed for Zn(T(*p*-CN)PP)$\cdot CHCl_3 \cdot C_6H_6$. In the Cu(II) porphyrin species, Cu(T(*p*-CN)PP)$\cdot 2C_6H_5NO_2$, cross-linking between adjacent chains is observed. The fourth bonding pattern utilizes ligand to metal coordination and is addressed subsequently (11).

Two clathrates of 5,10,15,20-tetra(4-carboxy)phenylporphyrin have been reported by Dastidar *et al.* (12) Interpenetrating networks in the 1:1 Zn(T(*p*-CO_2H)PP)$\cdot$ *sec*-phenethyl alcohol included material are formed when a porphyrin molecule hydrogen bonds to four other porphyrins via "typical" carboxylic acid dimer aggregation. A planar two-dimensional array is formed in this manner (Fig. 7). The

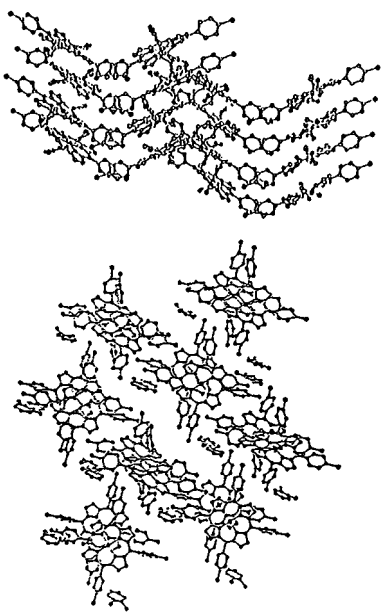

FIG. 7. Interporphyrin bonding, layered structure and cavities in Zn(T*p*CPP)$\cdot C_8H_{10}O$. Reprinted from P. Dastidar, Z. Stein, I. Goldberg, and C. E. Strouse, *Supramol. Chem.* **7,** 257 (1996), Copyright OPA, N.V., with permission from Gordon and Breach Publishers.

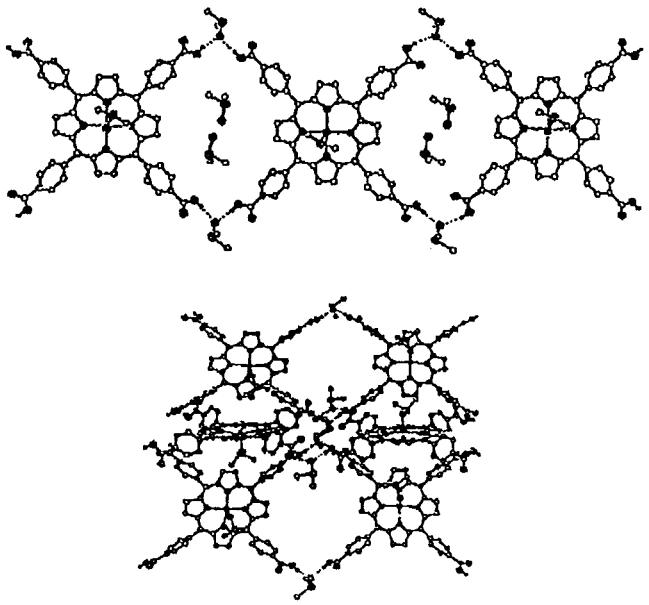

FIG. 8. Interporphyrin bonding and interpenetrating networks in Zn(TpCPP)$\cdot 3C_2H_6SO$. Reprinted from P. Dastidar, Z. Stein, I. Goldberg, and C. E. Strouse, *Supramol. Chem.* **7,** 257 (1996), Copyright OPA, N.V., with permission from Gordon and Breach Publishers.

sec-phenethyl alcohol is axially bound to the central zinc ion. Porphyrin macrocycles of parallel layers overlap and are interpenetrated by approximately perpendicular layers (dihedral angle $\sim 70°$). A "large central cavity of a rhombic shape" with dimensions $18 \times 16 \times 21$ Å is reported (12). This "cavity," however, is actually fully filled by two metalloporphyrins from perpendicular arrays. This example illustrates one of the challenges of creating porous extended frameworks: constructing noninterpenetrating networks.

The construction of Zn(T(*p*-CO_2H)PP)$\cdot 3C_2H_6SO$ (DMSO) is based on *cis*-side interaction of carboxylic acid groups with hydrogen bonding to a bridging DMSO molecule. This results in generation of a one-dimensional polymer chain reminiscent of that observed in Zn and Cu(T(p-OH)PP) networks (Fig. 6). Additional DMSO molecules bridge parallel polymeric chains, creating a two-dimensional array. An approximately perpendicular network intersects each layer. There are no hydrogen bonds between perpendicular layers (Fig. 8). A cavity of 6.5×10 Å is reported, and TGA results suggest loss of solvents in two steps (axially coordinated versus guest DMSO molecules) (12).

Suslick and coworkers explored supramolecular networks based on hydrogen bonding between symmetrically substituted octahydroxyporphyrins (13, 14). Both *ortho*- and *meta*-tetrakis(dihydroxyphenyl)porphyrins (Fig. 9) and their Zn(II) and Mn(III) derivatives were developed as molecular building blocks for nanoporous materials. The position of the peripheral hydroxyl groups, the choice of metalated or free base porphyrin, and the nature of the

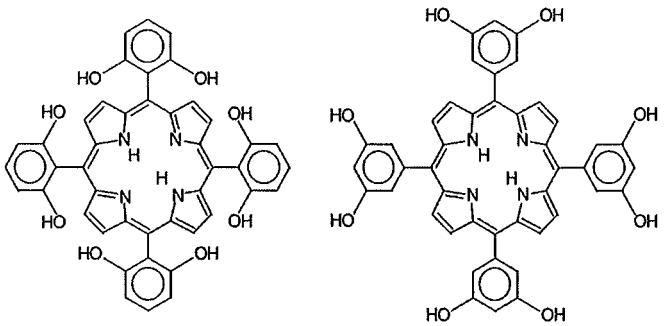

FIG. 9. 5,10,15,20-Tetrakis(2′,6′-dihydroxyphenyl)porphyrin, H_2(T(2′,6′-DHP)P), and 5,10,15,20-tetrakis(3′,5′-dihydroxyphenyl)porphyrin, H_2(T(3′,5′-DHP)P). Reprinted from P. Bhyrappa, S. R. Wilson, and K. S. Suslick, *Supramol. Chem.* **4,** 169 (1998), Copyright OPA, N.V., with permission from Gordon and Breach Publishers.

solvate dramatically influence structural features. These materials featured significant void volumes, as high as 67% calculated channel volume from X-ray crystal structures (Table 2).

A one-dimensional hydrogen-bonding structure was found for H_2(T(3′,5′-DHP)P)·5EtOAc in which porphyrin macrocycles stack in a columnar fashion. These columns of porphyrins align parallel to one another, forming a porous three-dimensional network with channels of 6.5×6.5 Å between them and 3.4×3.4 Å running perpendicular to the columns (Fig. 10). The stacked columns are held together by weak van der Waals interactions. When benzonitrile is used as the solvent species, the structure of H_2(T(3′,5′-DHP)P)·$7C_6H_5CN$ changes substantially to a two-dimensional array of porphyrins interconnecting via hydrogen bonds, generating a three-dimensional corrugated-sheet configuration. The observed variation in solid-state structure is credited to steric requirements necessitated by the larger benzonitrile guest molecules. Channels parallel to the corrugated layers with dimensions 5.5×6.0 Å and another set approximately perpendicular calculated to be 4.0×5.0 Å were identified.

Both the Zn(II) and Mn(II) derivatives of the *meta*-hydroxyl species featured three-dimensional hydrogen-bonded networks. Zn(T(3′,5′-DHP)P)$(THF)_2 \cdot 2THF \cdot 3CH_2Cl_2$ has an interconnected layer motif in which the metalloporphyrins are arranged in a "slipped stack" orientation (Fig. 11). In the structure of Mn(T(3′,5′-DHP)P)(Cl)·2EtOAc, the chloride anion bridges four hydroxyl groups from four separate porphyrins in a square planar arrangement with an average Cl···O distance of 3.01 Å creating a two-dimensional array (Fig. 12). Hydrogen bonding between layers generates a three-dimensional network with 4.6×3.4 Å-wide channels.

When the hydroxyl substituents are changed simply from the *meta*- to the *ortho*-phenyl positions, an essentially

TABLE 2
Channel Volumes for Various Porphyrin Complexes

Porphyrin complex	Z	Unit cell volume (Å^3)	Porphyrin volume/ unit cell[a] (Å^3)	Solvate volume/ unit cell[a] (Å^3)	Void volume/ unit cell[a] (Å^3)	Total channel volume/ unit cell[b] (Å^3)
H_2TPP[c]	1	801.9	590.8	0	211	211 [26.3%]
H_2T(3′,5′-DHP)P·5 EtOAc	1	1581	620.8	412.5	547.7	960.2 [60.7%]
H_2T(2′,6′-DHP)P·4 EtOAc	2	2770.9	1233.0	660	877.9	1537.9 [55.5%]
H_2T(3′,5′-DHP)P·$7C_6H_5CN$	2	3811	1241.6	1547	1022	2569.4 [67.4%]
Zn[T(2′,6′-DHP)P]$(EtOAc)_2$·2EtOAc	1	1387.2	804.1	168	415.2	583.2 [42.0%]
Zn[T(3′,5′-DHP)P]$(THF)_2 \cdot 3CH_2Cl_2 \cdot 2THF$	1	1597.6	755.8	326.9	514.8	841.7 [52.7%]
Mn[T(3′,5′-DHP)P]$(THF)_2 \cdot Cl^- \cdot 2THF \cdot 5\ C_6H_5CH_3$	2	4289	1612.2	1355	1321.8	2676.7 [62.4%]

Note. Reprinted with permission from P. Bhyrappa, S. R. Wilson, and K. S. Suslick, *J. Am. Chem. Soc.* **119,** 8492 (1997).

[a] Porphyrin and solvate van der Waals volumes were calculated from Quanta for each unit cell. Void volume is defined as the unit cell volume minus the sum of the porphyrin volume and the solvate volume. For the metalloporphyrins, the volumes of the coordinated ligands were counted as part of the porphyrin volume.

[b] Total channel volume is defined as the sum of void and solvate volume, in Å^3. Values in brackets refer to the percentage of total channel volume in the unit cell.

[c] Crystallographic data is taken from S. J. Silvers, A., Tulinsky, A. *J. Am. Chem. Soc.* **89,** 3331 (1967).

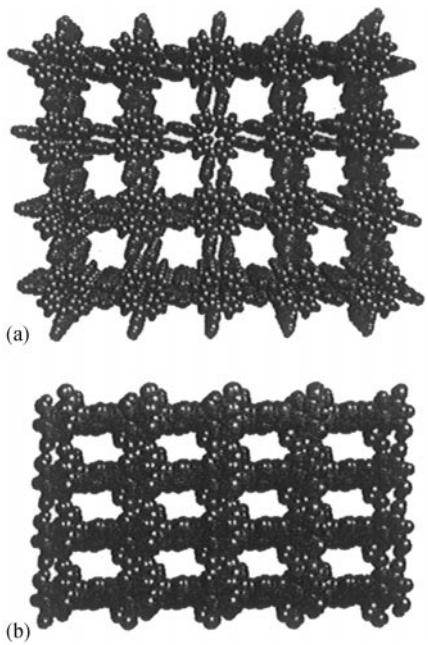

FIG. 10. Molecular packing diagrams of H_2(T(3′,5′-DHP)P)·5EtOAc showing (a) channels between porphyrins columns and (b) channels perpendicular to the columns. Reprinted with permission from P. Bhyrappa, S. R. Wilson, and K. S. Suslick, *J. Am. Chem. Soc.* **119,** 8492 (1997). Copyright 1997 American Chemical Society.

two-dimensional layered material results. The peripheral hydroxyl groups of H_2(T(2′,6′-DHP)P)·4EtOAc induce a slight ruffling of the porphyrin macrocyclic rings and show strong directional hydrogen bonding. The packing of the layers formed channels 3.0×3.6 Å wide (Fig. 13). A similar packing motif was observed for the Zn(II) metalloporphyrin species (13).

Recently, Sugiura *et al.* prepared, a layered material from *p*-methylthio- and *p*-methylseleno-tetraphenylporphyrins (15). These structures were stabilized by CH $\cdots \pi$ hydrogen bonds. Pendant *trans*-methyl groups interact with the ring π-system of the two neighboring porphyrin molecules, producing a two-dimensional network.

METAL ION COORDINATION NETWORKS

In the past decade, significant progress toward the rational construction of three-dimensional solids assembled from metal cations and organic molecules has been described (16, 17). Of particular interest have been metal–organic coordination networks possessing nanoscale pores (18). Metal–ligand interactions are often quite strong and should therefore provide a more robust framework than those based on van der Waals, hydrogen bonds, or π–π interactions.

Goldberg and coworkers have reported a number of inclusion compounds utilizing coordination of substituted tetraphenylporphyrins. Porphyrinic inclusion compounds of 5,10,15,20-tetra(4-pyridyl)porphyrin, H_2(TPyP), exhibited two general motifs (19). Crystallization of the Zn(TPyP) complex resulted in a geometry featuring "zig-zag" polymer chains in which the central Zn(II) ion is axially ligated by pyridyl substituent from an adjacent porphyrin. A similar arrangement was observed for inclusion compounds of aromatic solvents such as aniline. Only one pyridyl moiety per porphyrin building block coordinates to another porphyrin, thereby limiting ligand–metal interactions to one-dimensional polymeric chains. The guest species is located in a cavity adjacent to the pyridyl substituent *trans*- to the pyridyl axially ligating the metal center of an adjacent porphyrin in the zig-zag chain.

Inclusion compounds in tetrapyridylporphyrin systems of methanol and water induce three-dimensional coordination

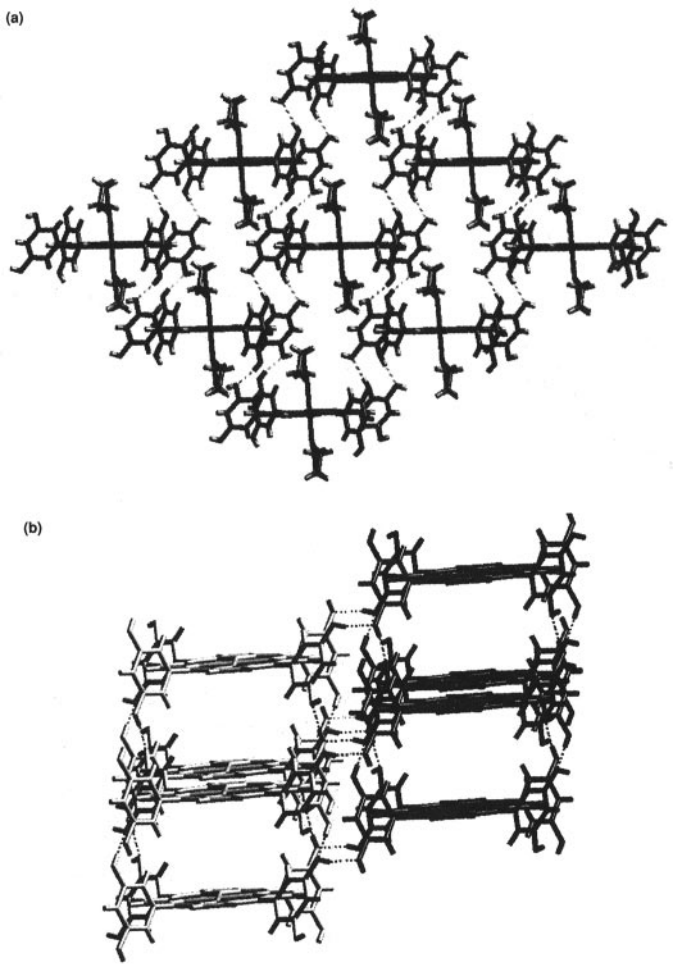

FIG. 11. (a) Two-dimensional layer from the crystal structure of Zn(T(3′,5′-DHP)P)$(THF)_2 \cdot 2THF \cdot 3CH_2Cl_2$. (b) Molecular packing diagram showing interconnected layers. Porphyrins in dark and light shades indicate two different layers. Dotted lines indicate hydrogen-bonding interactions. Noncoordinated solvates are omitted for clarity. Reprinted with permission from P. Bhyrappa, S. R. Wilson, and K. S. Suslick, *J. Am. Chem. Soc.* **119,** 8492 (1997). Copyright 1997 American Chemical Society.

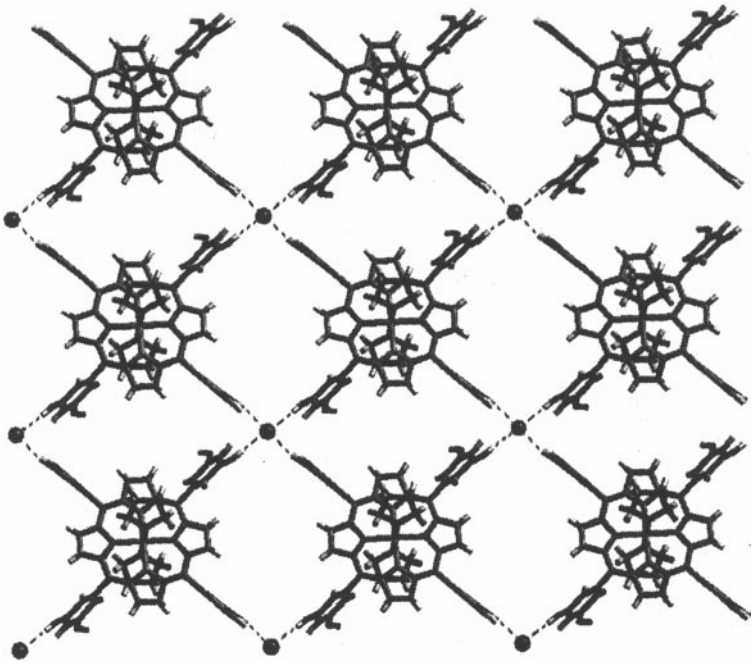

FIG. 12. Molecular packing diagram of $Mn(T(3',5'\text{-DHP})P)(THF)_2 \cdot Cl \cdot 2THF \cdot 5C_6H_5CH_3$ showing two-dimensional sheets of porphyrin linked by unusual square-planar Cl^- anions hydrogen bonding to four metalloporphyrins. Spheres indicate bridging chloride ions. Solvate molecules and coordinated THF ligands omitted for clarity. Reprinted with permission from P. Bhyrappa, S. R. Wilson, and K. S. Suslick, *J. Am. Chem. Soc.*, **119,** 8492 (1997). Copyright 1997 American Chemical Society.

polymers and typify a second motif encountered. *Trans*-pyridyl substituents on a Zn(TPyP) were observed to ligate axially the metal centers of adjacent porphyrin moieties generating a polymeric chain in one dimension. Cross-linking in a second dimension occurs when the original porphyrin molecule is coordinated by two pyridyl moieties from two additional porphyrin molecules. The two remaining pyridyl groups participate in hydrogen bonding with included water molecules. An intricate three-dimensional framework results (Fig. 14).

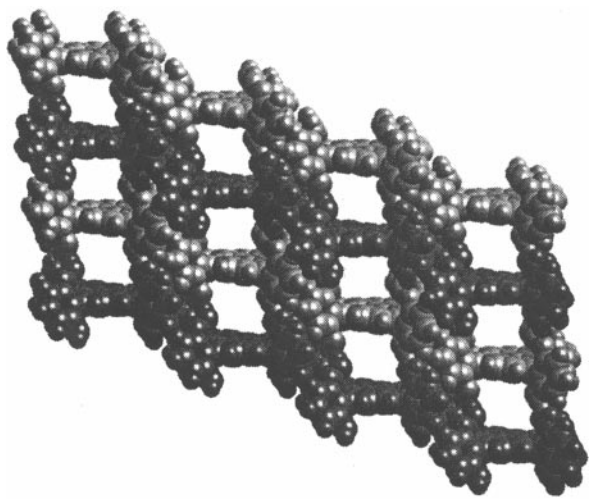

FIG. 13. Molecular packing diagram of $H_2(T(2',6'\text{-DHP})P) \cdot 4EtOAc$ showing channels between the porphyrin layers. Solvent molecules are omitted for clarity. Reprinted with permission from P. Bhyrappa, S. R. Wilson, and K. S. Suslick, *J. Amer. Chem. Soc.* **119,** 8492 (1997). Copyright 1997 American Chemical Society.

For inclusion solids of 5,10,15,20-tetra(4-cyano)phenylporphyrin, $H_2(T(p\text{-CN})PP)$, one of the four structural motifs encountered by Goldberg involved ligand to metal interactions (11). Two-dimensional coordination networks similar to those observed for Zn(TPyP) materials were found in $Zn(T(p\text{-CN})PP) \cdot 2C_6H_5NO_2$ (nitrobenzene), $Zn(T(p\text{-CN})PP) \cdot CHCl_3$ (chloroform), and $Zn(T(p\text{-CN})PP) \cdot C_7H_8O$ (anisole) materials. The guest species intercalate between the porphyrin layers.

Attempting to mimic the topology of the PtS structure, Robson and coworkers explored metal to ligand coordinative bonding as means of building more robust porphyrinic materials. They reported a structure in which Pd(TPyP) molecules are interconnected by Cd(II) centers (20). Each porphyrin is coordinated by two *trans* pyridyl donor porphyrin molecules and by two *cis* donor porphyrin molecules (Fig. 15). The overall neutral framework $[Pd(TPyP) \cdot Cd(NO_3)_2 \cdot 8.6H_2O]$ features infinite interwoven layers of the porphyrin network.

In subsequent work, Robson and coworkers (21) reported three-dimensional network solids using the copper porphyrin complexes of 5,10,15,20-tetra-4′-pyridylporphyrin, Cu(TPyP), and 5,10,15,20-tetra-4′-cyanophenylporphyrin, Cu(T(*p*-CN)PP). Large extended channels (10–20 Å) were

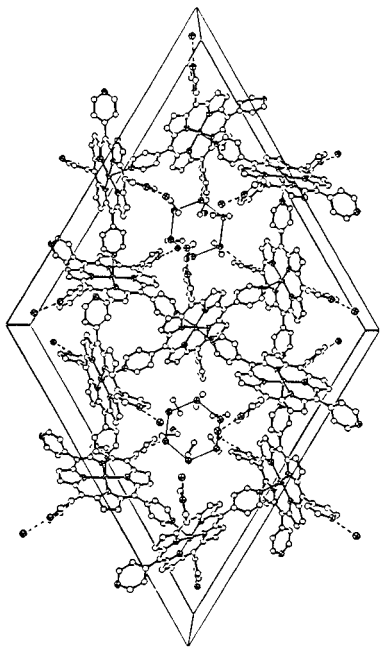

FIG. 14. Crystal structure of $Zn(TPyP)\cdot CH_3OH\cdot 2H_2O$. The marked hexagons indicate hydrogen-bonding interactions between six water molecules and pyridyl groups of porphyrins in adjacent unit cells. Reprinted from H. Krupitsky, Z. Stein, and I. Goldberg, *J. Incl. Phenom. Mol. Recog. Chem.* **18,** 177 (1994), Copyright Kluwer Academic Publishers, with kind permission from Kluwer Academic Publishers.

observed in which tetrahedral Cu(I) ions (as opposed to the square planar Cu(II) ions bound to the center of the porphyrin ring) coordinate to pyridyl or cyano groups on the

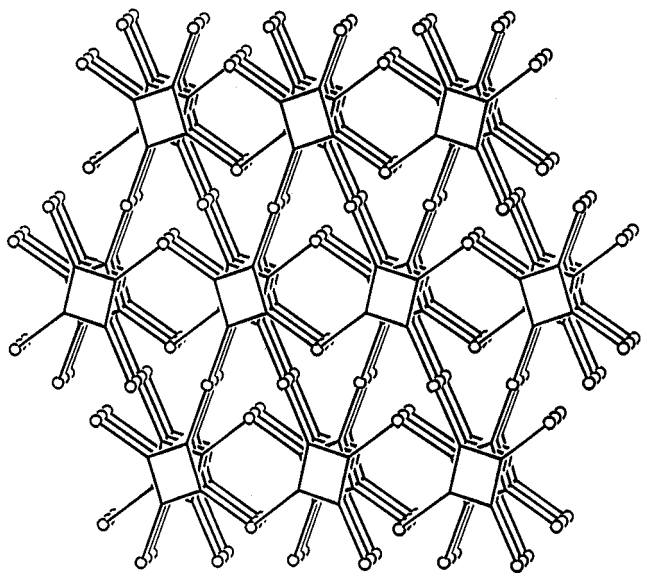

FIG. 15. Schematic illustration of three-dimensional porphyrin network in $Pd(TPyP)\cdot Cd(NO_3)_2\cdot 8.6H_2O$ in which porphyrins are represented as squares and cadmium ions as circles. Solvent molecules are omitted for clarity. Reprinted with permission from B. F. Abrahams, B. F. Hoskins, and R. Robsin, *J. Am. Chem. Soc.* **113,** 3606 (1991). Copyright 1991 American Chemical Society.

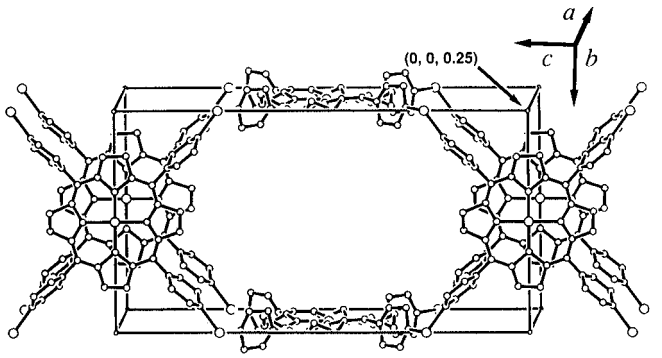

FIG. 16. Packing arrangement in $[Cu(TPyP)\cdot Cu]_n^{n+}$ framework showing single independent net. Larger circles represent copper ions. Solvent and noncoordinating anions omitted for clarity. Reprinted with permission from B. F. Abrahams, B. F. Hoskins, D. M. Michall, and R. Robson, *Nature* **369,** 727 (1994). Copyright 1994 Macmillan Publishers Ltd. http://www.nature.com.

periphery of four porphyrin molecules. While the cationic frameworks were reported to occupy less than half the volume of the crystal, the void spaces were occupied by noncoordinating anions (BF_4^-) and highly disordered solvent molecules (acetonitrile/nitrobenzene); upon removal of the anions, crystallinity was lost. In the tetrapyridyl system, a single infinite PtS-like network was discovered (Fig. 16). In contrast, the tetracyanophenylporphyrin system has two independent interpenetrating networks, each geometrically identical to single independent tetrapyridylporphyrin framework, were delineated. The tetrahedral Cu(I) ions in the tetrapyridylporphyrin system are located closer to the large pyridyl ring, which sterically restricts the inclusion of another independent network.

Anionic functional groups on the organic molecules can circumvent the problems of a charged framework. Suslick and coworkers have explored the use of carboxylic acid-substituted porphyrins for building microporous porphyrinic solids. Tetraphenylporphyrins with carboxylate functionalities, i.e., 5,10,15,20-*tetra*-(4-carboxy)phenylporphyrin, $H_2(T(pCO_2H)PP)$, and 5,10,15,20-*tetra*-(3,5-dicarboxy)phenylporphyrin, $H_2(T(3,5\text{-}CO_2H)PP)$ (22), were selected as organic precursors. The carboxylic acids serve to solubilize of the large porphyrin molecules and, when deprotonated, to provide an anionic site for coordination of cationic metal atoms. A tightly packed and interpenetrated, linear polymeric array was observed in the solid-state structure of the free base *p*-carboxylate porphyrin with Ca(II) bridging centers (Fig. 17). Hydrogen bonding between coordinated water molecules in the calcium layers was observed to stabilize the three-dimensional structure (23). The independent linear polymers are structurally similar to those observed for the T(*p*-OH)PP hydrogen bonded networks by Strouse and coworkers (Fig. 6). Porous network material of the Co(III) and Mn(III) derivatives of *p*-carboxylate porphyrin have been characterized by X-ray crystallography

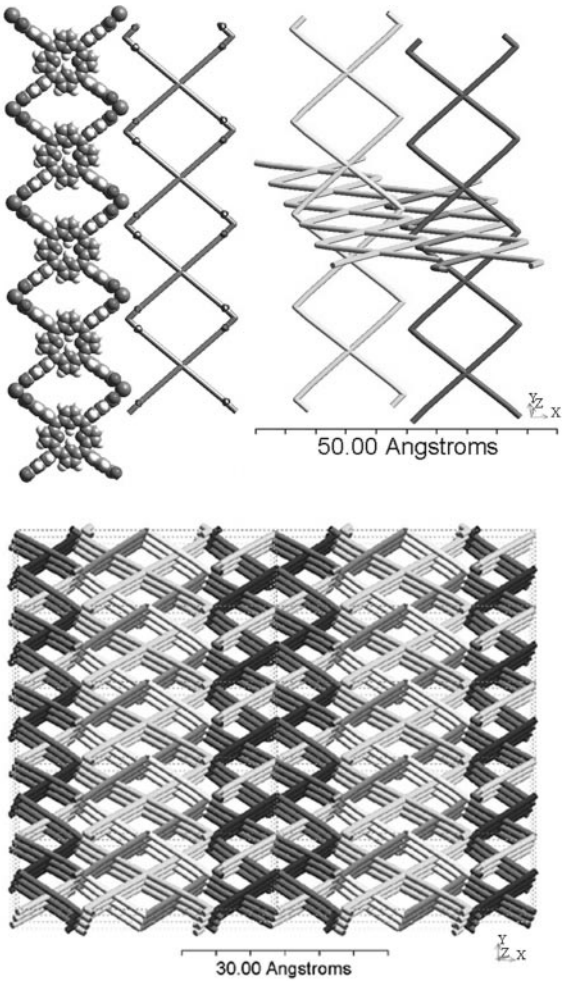

FIG. 17. Parallel polymeric porphyrin bands showing coordination between the four bidentate porphyrin carboxylates and calcium ions as both space filling and schematic models. In this schematic model, intersection of cylinders represents center of porphyrin macrocycle and corners represent calcium ions. Guest pyridine molecules and coordinated water molecules omitted for clarity. M. E. Kosal, J. H. Chou, and K. S. Suslick, in preparation.

and gas adsorption studies. These materials have demonstrated retention of structural features and microporosity upon removal of guest molecules (24). The tetrakis(di-*meta*-carboxyphenyl)porphyrin, H_2(T(3,5-CO_2H)PP), is anticipated to produce three-dimensional network structures due to the geometrical orientation of the carboxylic acid groups. In the crystal structure of the free base porphyrin, channels were observed to form in the stacked packing of the discrete porphyrin molecules (Fig. 18) (22).

A similar basic structural motif of interpenetrating linear arrays was recently elucidated by Noll and Wang using H_2(TPyP) in which the pyridine nitrogen atoms coordinated to $HgBr_2$ moieties (25). They describe the formation of one-dimensional, noninterpenetrating, linear coordination polymers in which there is a cavity 8.4×3.7 Å between adjacent porphyrins in each polymer. Guest chloroform molecules are reported to reside between porphyrin chains rather than as included species within the cavities. Rapid loss of $CHCl_3$ guests and crystallinity nature upon removal from the mother liquor was noted.

In exciting recent work by Lin (26), a more robust porphyrin network has been constructed using Co(II) and Mn(II) tetrapyridylporphyrin building blocks. Featuring a layered framework of overlapping hexameric cages, they report an infinite channel along one crystallographic axis with a pore size of 13×16 Å based on van der Waals radii of atoms lining the channel. As demonstrated by TGA, the channel is initially occupied by highly disordered solvent molecules, which can be removed upon heating. To draw further the parallel to inorganic zeolites, the pore size was determined to be 5.8 Å by N_2 adsorption/desorption (Fig. 19).

SILOXANE NETWORKS

Mansuy and coworkers employed the techniques of sol–gel chemistry in order to synthesize a hybrid organic–inorganic network material from 5,10,15,20-tetrakis (2,3,4,5,6-pentafluoro)phenylporphyrin, M(T(F_5P)P) with $M = H_2$, Fe^{III}, or Mn^{III}) and 3-aminopropyltriethoxysilane (APTES) building blocks (Fig. 20). The resulting "metalloporphyrinosilicas," porphyrin-bridged polysilsesquioxanes, were employed as solid catalysts for alkene epoxidation and alkane hydroxylation (27). An attempt to design cavities of specific size and shape in similar Fe(III)porphyrinosilica networks was pursued by Ciuffi *et al.* (28). Axially coor-

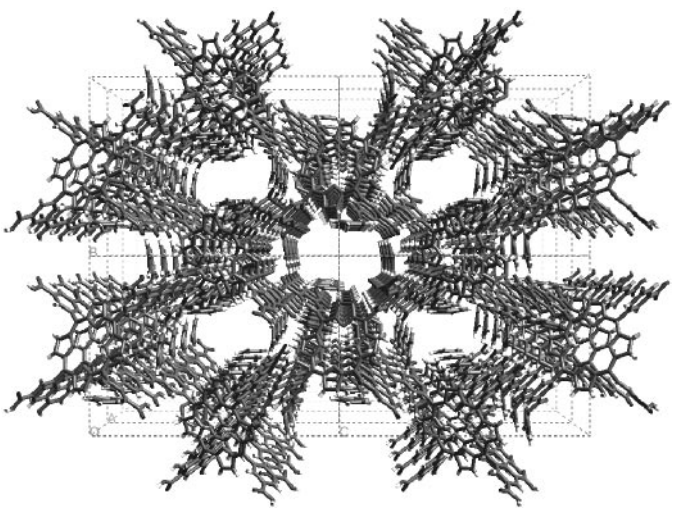

FIG. 18. Crystal packing in H_2(DiCarPP) molecular species showing channels between porphyrin columns. Solvent molecules omitted for clarity. Reprinted with permission from B. Patel, "Porphyrin Liquid Crystals," Department of Chemistry, Univ. of Illinois at Urbana—Champaign, Urbana, IL, 1996.

dinated nitrogenous bases (imidazole, 1-methylimidazole, 2-ethylbenzimidazole, 4-phenylimidazole, or miconazole) were utilized as template molecules. Removal of the template molecules was characterized by thermogravimetric analysis (TGA) of the solids.

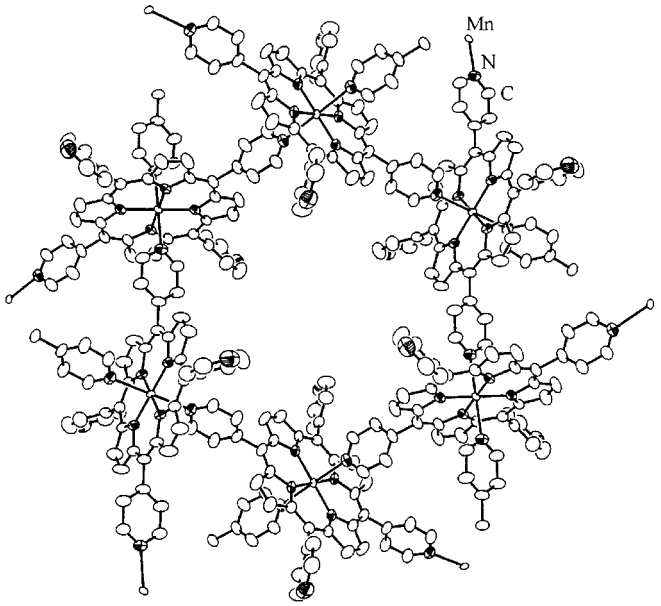

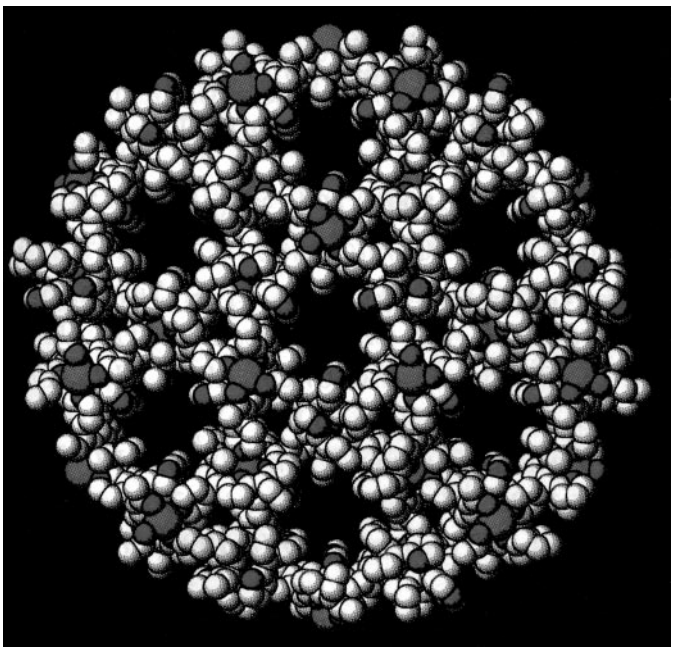

FIG. 19. Hexameric coordination motif observed in Co(TPyP)·guest and Mn(TPyP)·guest networks forming a 17×20-Å channel along the crystallographic c axis. (a) ORTEP plot along the threefold c axis (50% probability ellipsoids) of a single cage. (b) Perspective view of the open framework structure in a space filling representation. Hydrogen atoms and solvate molecules are omitted for clarity. Reprinted from K-J Lin, *Angew. Chem. Int. Ed.* **38,** 2730 (1990), with permission from Wiley–VCH.

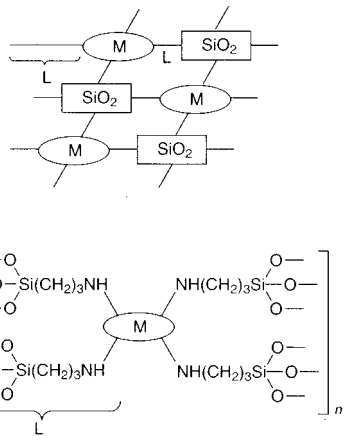

FIG. 20. Schematic of metalloporphyrinosilica network, in which ovals represent porphyrin macrocyclic rings. Reprinted from P. Battioni, M. Louloudi, B. Schollhorn, G. A. Spyroulias, D. Mansuy, and T. G. Traylor, *Chem. Commun.* 2037 (1996), with permission from The Royal Society of Chemistry.

CONCLUSIONS

From this survey of the microporous solid state structures of porphyrins and metalloporphyrins, it is clear that many structures contain substantial volumes of solvates or clathrates in molecularly sized channels or cavities. A diverse range of extended frameworks have been discovered, held together by van der Waals interactions, hydrogen bonding, or metal coordination. The facile functionality available at the periphery of porphyrins, combined with their intrinsic chemical and thermal stability, continues to provide endless opportunities for crystal engineering.

There are problems in the definition of porosity for some of these structures. In some cases, authors have been rather generous in claiming porosity in their structures, which in fact are fully packed with interpenetrating networks. In other cases, as true with most so-called "porous" solids based on molecular building blocks, the porosity tends to be one-way only: if the solvates are removed, the structure collapses irreversibly. This is especially problematic for solids held together by van der Waals and hydrogen-bonding interactions. As has been noted before, at least for molecular solids, nature abhors a vacuum!

It is fair to say that in this field two major goals have not yet been fulfilled. First, reversible and selective absorption of molecules into a zeolitic-like porphyrin solid remains unrealized. Second, and more importantly, the use of metalloporphyrin solids as shape- or size-selective heterogeneous catalysts, especially for oxidative processes, has yet to be achieved.

REFERENCES

1. K. S. Suslick, "Comprehensive Supramolecular Chemistry: Bioinorganic Systems," Elsevier, Oxford, 1996.

2. B. Meunier, *in* "Metalloporphyrins Catalysed Oxidations" (F. Monanari and L. Casella, Eds.), p. 1. Kluwer Academic, Boston, 1994.
3. K. S. Suslick and S. Van Deusen-Jeffries, *in* "Comprehensive Supramolecular Chemistry: Bioinorganic Systems" (K. S. Suslick, Ed.), Vol. 5, p. 733. Elsevier Science, Oxford, 1996.
4. M. P. Byrn, C. J. Curtis, S. I. Khan, P. A. Sawin, R. Tsurumi, and C. E. Strouse, *J. Am. Chem. Soc.* **112,** 1865 (1990).
5. M. P. Byrn, C. J. Curtis, I. Goldberg, Y. Hsiou, S. I. Khan, P. A. Sawin, S. K. Tendick, and C. E. Strouse, *J. Am. Chem. Soc.* **113,** 6549 (1991).
6. M. P. Byrn, C. J. Curtis, Y. Hsiou, S. I. Khan, P. A. Sawin, S. K. Tendick, A. Terzis, and C. E. Strouse, *J. Am. Chem. Soc.* **115,** 9480 (1993).
7. H. Krupitsky, Z. Stein, and I. Goldberg, *J. Incl. Phenom. Mol. Recog. Chem.* **20,** 211 (1995).
8. I. Goldberg, H. Krupitsky, Z. Stein, Y. Hsiou, and C. E. Strouse, *Supramol. Chem.* **4,** 203 (1995).
9. P. Dastidar and I. Goldberg, *Acta Crystallogr.* **C52,** 1976 (1996).
10. D. Philip and J. F. Stoddart, *Angew. Chem. Int. Ed. Engl.* **35,** 1154 (1996).
11. R. K. Kumar, S. Balasubramanian, and I. Goldberg, *Inorg. Chem.* **37,** 541 (1998).
12. P. Dastidar, H. Krupitsky, Z. Stein, and I. Goldberg, *J. Incl. Phenom. Mol. Recog. Chem.* **24,** 241 (1996).
13. P. Bhyrappa, S. R. Wilson, and K. S. Suslick, *J. Am. Chem. Soc.* **119,** 8492 (1997).
14. P. Bhyrappa and K. S. Suslick, *Supramol. Chem.* **9,** 169 (1998).
15. K. Sugiura, K. Ushiroda, T. Tanaka, M. Sawada, and Y. Sakata, *Chem. Lett.* 927 (1997).
16. R. Robson, *in* "Solid-State Supramolecular Chemistry: Crystal Engineering" (D. D. MacNicol, F. Toda, and R. Bishop, Eds.), Vol. 6, p. 733, Pergamon, New York, 1996.
17. C. L. Bowes and G. A. Ozin, *Adv. Mater.* **8,** 13 (1996).
18. O. M. Yaghi, H. Li, C. Davis, D. Richardson, and T. L. Groy, *Acc. Chem. Res.* **1998,** 474 (1998).
19. H. Krupitsky, Z. Stein, and I. Goldberg, *J. Incl. Phenom. Mol. Recog. Chem.* **18,** 177 (1994).
20. B. F. Abrahams, B. F. Hoskins, and R. Robsin, *J. Am. Chem. Soc.* **113,** 3606 (1991).
21. B. F. Abrahams, B. F. Hoskins, D. M. Michall, and R. Robson, *Nature* **369,** 727 (1994).
22. B. Patel, "Porphyrin Liquid Crystals," Department of Chemistry, Univ. of Illinois at Urbana—Champaign, Urbana, 1996.
23. M. E. Kosal, J. H. Chou, and K. S. Suslick, in preparation.
24. J. H. Chou, M. E. Kosal, and K. S. Suslick, in preparation.
25. L. Pan, B. C. Noll, and X. Wang, *Chem. Commun.* 157 (1998).
26. K.-J. Lin, *Angew. Chem. Int. Ed.* **38,** 2730 (1999).
27. P. Battioni, M. Louloudi, B. Schollhorn, G. A. Spyroulias, D. Mansuy, and T. G. Traylor, *Chem. Commun.* 2037 (1996).
28. K. J. Ciuffi, H. C. Sacco, J. B. Valim, C. Manso, M.C.P., O. A. Serra, O. R. Nascimento, E. A. Vidota, and Y. Iamamoto, *J. Non-Cryst. Solids* **247,** 146 (1999).